



## 3-D models and structural analysis of rock avalanches: the study of the deformation process to better understand the propagation mechanism

Céline Longchamp<sup>1</sup>, Antonio Abellan<sup>1</sup>, Michel Jaboyedoff<sup>1</sup>, and Irene Manzella<sup>2</sup>

<sup>1</sup>Institute of Earth Sciences, University of Lausanne, Switzerland

<sup>2</sup>Department of Earth Sciences, University of Geneva, Switzerland

*Correspondence to:* C. Longchamp (celine.longchamp@unil.ch)

Received: 22 October 2015 – Published in Earth Surf. Dynam. Discuss.: 10 November 2015

Revised: 22 July 2016 – Accepted: 19 August 2016 – Published: 28 September 2016

**Abstract.** Rock avalanches are extremely destructive and uncontrollable events that involve a great volume of material ( $> 10^6 \text{ m}^3$ ) and several complex processes, and they are difficult to witness. For this reason the study of these phenomena using analog modeling and the accurate analysis of deposit structures and features of laboratory data and historic events become of great importance in the understanding of their behavior.

The main objective of this research is to analyze rock avalanche dynamics and deformation process by means of a detailed structural analysis of the deposits coming from data of 3-D measurements of mass movements of different magnitudes, from decimeter level scale laboratory experiments to well-studied rock avalanches of several square kilometers' magnitude.

Laboratory experiments were performed on a tilting plane on which a certain amount of a well-defined granular material is released, propagates and finally stops on a horizontal surface. The 3-D geometrical model of the deposit is then obtained using either a scan made with a 3-D digitizer (Konica Minolta VIVID 9i) or a photogrammetric method called structure from motion (SfM), which requires taking several pictures from different point of view of the object to be modeled.

In order to emphasize and better detect the fault structures present in the deposits, we applied a median filter with different moving window sizes (from  $3 \times 3$  to  $9 \times 9$  nearest neighbors) to the 3-D datasets and a gradient operator along the direction of propagation.

The application of these filters on the datasets results in (1) a precise mapping of the longitudinal and transversal displacement features observed at the surface of the deposits and (2) a more accurate interpretation of the relative movements along the deposit (i.e., normal, strike-slip, inverse faults) by using cross sections. Results show how the use of filtering techniques reveals disguised features in the original point cloud and that similar displacement patterns are observable both in the laboratory simulation and in the real-scale avalanche, regardless the size of the avalanche. Furthermore, we observed how different structural features, including transversal fractures and folding patterns, tend to show a constant wavelength proportional to the size of the avalanche event.

## 1 Introduction

Rock avalanches, or sturzstroms (Heim, 1932), are defined as an extremely rapid, massive, flow-like motion of fragmented rocks derived from a bedrock failure (Hungr et al., 2001). Rock avalanches are events in which granular masses of rock debris flow at high speeds, commonly with unusual runout (Corominas, 1996; Friedmann and Losert, 2003). A great volume of material ( $> 10^6 \text{ m}^3$ ) is involved, and the flowing mass can reach velocities on the order of tens of meters per second. They can travel long distances, on the order of kilometers, and cover an area over  $0.1 \text{ km}^2$  (Hsü, 1975). They present a very high mobility and need to be simulated with adapted frictional models (Hungr et al., 2001; Pedrazzini et al., 2012). Authors have proposed different possible causes, which could explain the high mobility of these phenomena, such as the influence of the large destabilized volume (Heim, 1932; Hsü, 1975; Scheidegger, 1973; Nicoletti and Sorriso-Valvo, 1991), the momentum transfer within the rear and the front of the flowing mass (Van Gassen and Cruden, 1989; Manzella and Labiouse, 2009), or the fragmentation of the spreading mass (Heim, 1932; Davies, 1982; Davies and McSaveney, 1999; Locat et al., 2006). In order to understand the behavior of such granular flows, laboratory scale experiments provide important information on their propagation and on the parameters influencing their mobility, even if they reproduce idealized conditions (Davies and McSaveney, 1999, 2003; McDougall and Hungr, 2004; Shea and van Wyk de Vries, 2008; Manzella and Labiouse, 2008, 2009; Longchamp 2016). Dufresne (2012) highlighted that substrate material with the least frictional resistance showed the greatest response to granular flow, producing the longest runout. In their work, Andrade et al. (2010) and Paguican et al. (2014) studied analog flank collapse and highlighted that hummocks can form horst-and-graben structures during lateral spreading. Several authors have proposed different parameters for the geometrical description of large landslides. One of the most used is the *Fahrböschung* concept, which was introduced by Heim (1932) to estimate the maximum runout of rock avalanches or landslides (Scheidegger, 1973; Hsü, 1975; Davies, 1982) and which is defined as the angle of the straight line connecting the head of the scar to the end of the deposit.

Faults and folds are common features on the surface of rock avalanche deposits. One of the best examples is the rock avalanche deposit of Socompa Volcano (northern Chile). This deposit has been widely studied previously (Francis et al., 1985; van Wyk de Vries et al., 2001; Kelfoun and Druitt, 2005; Shea and van Wyk de Vries, 2008) and presents a well-preserved morphology thanks to the local arid climate. A complex assemblage of surface structures (normal faults, strike-slip faults, thrusts, ridges) is displayed on the surface of the deposit. Van Wyk de Vries et al. (2001) showed that these structures incise deeply the internal part of the deposit. The non-volcanic deposit of Blackhawk (California, USA)

also presents similar features (Shea and van Wyk de Vries, 2008) (Fig. 1a), as does the Frank Slide in Alberta (Canada) (Cruden and Hungr, 1986, 2011; Charrière et al., 2015). Features perpendicular to the flow direction are mainly present in the distal part of the deposit and are interpreted as the surface expression of the underneath topography. Reversibly, longitudinal features on the proximal and the central part of the deposit are assumed to be morphological features that were created during the process of avalanche propagation and deposition. It is also interesting to highlight that similar features have been observed on other planets, such as in Olympus Mons (Mars) (Fig. 1b). Shea and van Wyk de Vries (2008) provided a detailed map of this extraterrestrial Martian rockslide avalanche where it can be observed that thrust faults are located in the front of the deposit and are cut by strike-slip faults. Normal faults are presented in the central part of the deposit. Although these features occur during the emplacement of the deposit, few studies focus on these deformational settings. In their small-scale experiments, Dufresne and Davies (2008) showed that lateral levees developed where flows were parallel to the confining, whereas compressional ridge formed in response to declination in the front of the deposit.

In the present paper a detailed structural analysis is carried out based on data coming from dedicated laboratory experiments and historic events in order to better understand the deformation of these complex phenomena. Moreover, this research attempted to propose a simple methodology to describe and map the features at the surface of the deposits in order to provide information on the mobility of the rock avalanche.

## 2 Experimental methods

The first step of this study consisted in carrying out laboratory experiments in order to study the influence of a series of parameters on the features and structure of granular flow deposits. The experimental setup (see Fig. 2) consisted of a simple aluminum slope geometry composed of two distinct parts: a  $90 \times 70 \text{ cm}$  slope with an inclination ( $\alpha$ ) which can be precisely modified, connected with a curved part to a  $120 \text{ cm}$  long horizontal surface. Furthermore, the experimental setup also includes a box ( $11 \times 8 \times 7 \text{ cm}$ ) where the loose material is enclosed at the beginning of the experiment. This box, separated from the main setup, can be leaned against the slope and quickly separated from it by means of a retractile jack. This allows placing a precise quantity of granular material on the slope and releasing it, avoiding any vibrations. Experiments then consist in letting the mass propagate without lateral confinements till it reaches a complete stop (Fig. 2). As loose material is used, partial mixing of grains is observed. The fragmentation of layers is not taken into account in this study.

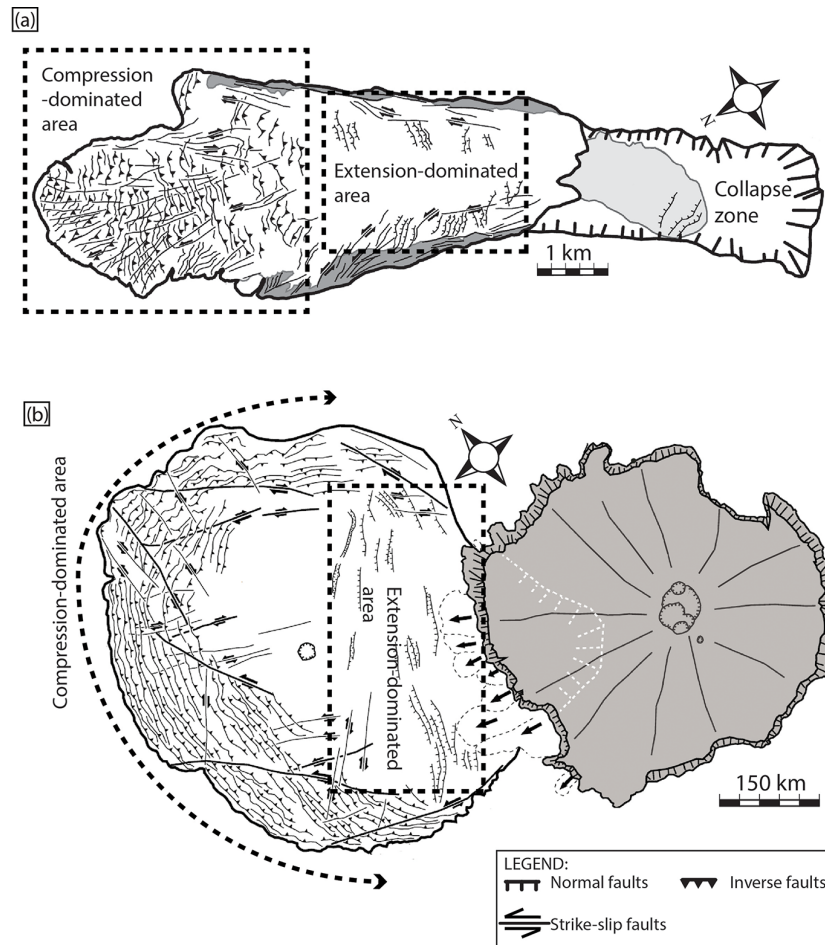


**Figure 1.** (a) Blackhawk deposit and (b) Martian deposit (modified after Shea and van Wyk de Vries, 2008).

Two different materials were used for the experiments: (a) the first type of material corresponds to angular and calibrated carborundum sand ( $\text{SiC}$ , density =  $3.21 \text{ g cm}^{-3}$ ) with three different grain sizes (Table 1). The choice of carborundum was made in order to avoid the characteristic electrostatic effects that have been often observed in granular flow experiments and that are not present in real events (Iverson and Denlinger 2001; Manzella, 2008). Furthermore, the angular shape of this type of material has close resemblances with natural material; (b) the second material corresponds to colored sands of similar grain size (Table 1). The choice of this material was driven by the need to observe the evolution of the initial stratigraphy, i.e., to analyze the deposit stratigraphy (given by different layers of different colors) during motion and emplacement of the mass.

The slope and the surface of deposition were artificially roughed by adding sandpaper, also made of carborundum sand, where the grain diameter has been varied. The basal friction  $\mu$  angle for each sandpaper was estimated by means of a dynamometer, and the results are given in Table 2.

**Table 1.** Characteristics of the material used.

Grading		Mean grain size ( $\mu\text{m}$ )	Range ( $\mu\text{m}$ )
Coarse	F10	2605	2830–2380
Medium	F36	545	590–500
Fine	F120	115	125–105
Colored	–	500	–

No scaling calculations were applied for this work, but we based our value for the slope, height of fall, and grain size for the laboratory on the work of Shea and van Wyk de Vries (2008). All the experiments were carried out with a constant volume within the same experiment ( $400 \text{ cm}^3 < V < 500 \text{ cm}^3$ ) and same height of fall for the granular material (50 cm). The runout of dry granular flow is influenced by the slope angle: the runout distance is greater for higher slope angle (Longchamp, 2016). For this study, a slope angle of  $40^\circ$  is chosen to better compare the results.

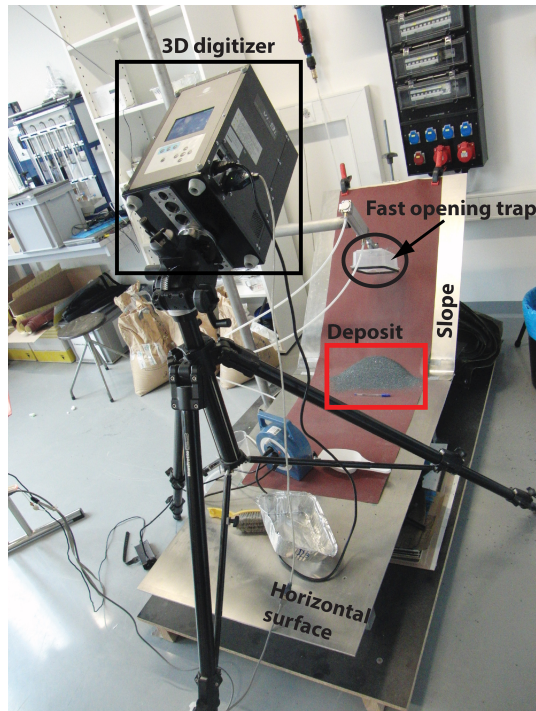


Figure 2. Laboratory setup.

The experiments were recorded by a high-speed camera (30 fps for a resolution of  $640 \times 480$ ); the final deposit was scanned by a 3-D digitizer (Konica Minolta VIVID 9i micro-lidar with a resolution of 30 000 points per point cloud, Fig. 2) and photographed. Finally a transparent separation was placed carefully along the major longitudinal section, and the material on one side was removed so that it was possible to observe the internal structure of the mass. In order to observe the repartition of the colored sand grains within the deposit, sand grains were counted at crucial sections along the deposit. For each measurement, a section of 0.2 cm length and a height corresponding to the thickness of the deposit was determined. In this section, the number of colored grains was manually counted. This gave further information on the different regimes affecting the flow and allowed for better constraint of the different part of the deposit that are affected by different regimes. Ten measurements were made along the deposit and cumulated.

In order to have significant results, three experiments were carried out with equal initial conditions.

### 3 Methodology

As mentioned above, during the propagation, the motion of the granular mass is recorded by a high-speed camera in order to analyze the deformation and spreading during the flow. Once the mass stopped, the first step was to take pictures of the deposit in order to study and inventory the visible longi-

Table 2. Characteristics of the different substrata.

Sand	Grit	Grain size ( $\mu\text{m}$ )	$\mu$ ( $^\circ$ )
Coarse	60	269	58.62
	120	125	48.67
Medium	320	46.2	43.17
	600	25.8	39.88
Fine	1200	15.3	34.13
	2500	8.4	33.40
Colored	–	42,5	44.79

tudinal and transversal features on the surface. The acquisition of a 3-D dataset was made using either a laser scanner (Konica Minolta VIVID 9i micro-lidar) or a photogrammetry technique, named structure from motion (SfM) (Westboy, 2012). The laser scanner technique is useful for scanning the deposit resulting from the propagation of carborundum sand, but the density of points is quite low (30 000 points per point cloud) (see Fig. 3b). Moreover, the setup is quite difficult to install, and the data take a long time to process. SfM differs fundamentally from conventional photogrammetry, in that the geometry of the scene, camera positions and orientation is solved automatically without the need to specify a priori a network of targets which have known 3-D positions (Westboy, 2012). Instead, these parameters are solved simultaneously using a highly redundant, iterative bundle adjustment procedure, based on a database of features automatically extracted from a set of multiple overlapping images (Westboy, 2012). Structure from motion is a simple technique requiring little material and is cheaper compared to lidar. The density of points is high (1 000 000 points per point cloud). This density of points allows identifying finer features on the deposit. The main disadvantage of this technique is that the post-processing of the data is sensitive to all variation in the images. Therefore, SfM cannot be applied to experiments with carborundum sand as the grains reflect the light with different intensity according to where the pictures is taken, and it could only be applied to the colorized sand deposit (Fig. 4). When the carborundum deposit is scanned by lidar, no problems of reflection were observed, whereas the photogrammetry gave a noisy point cloud. We applied the photogrammetry to the colored sand to have high-resolution point clouds and way more points compared to the lidar. Thanks to the use of different filtering techniques and operators, we were able to highlight the structural fingerprints on the deposit surface. This computational work aimed to highlight the features that cannot be observed by the naked eye, as follows:

#### (a) Application of a median filter technique

Data acquisition using a 3-D digitizer or SfM leads to a “noisy” surface in which the features to be detected are masked due to the scattering of the 3-D points around the real surface (Fig. 5a). To remove the noise, smooth-



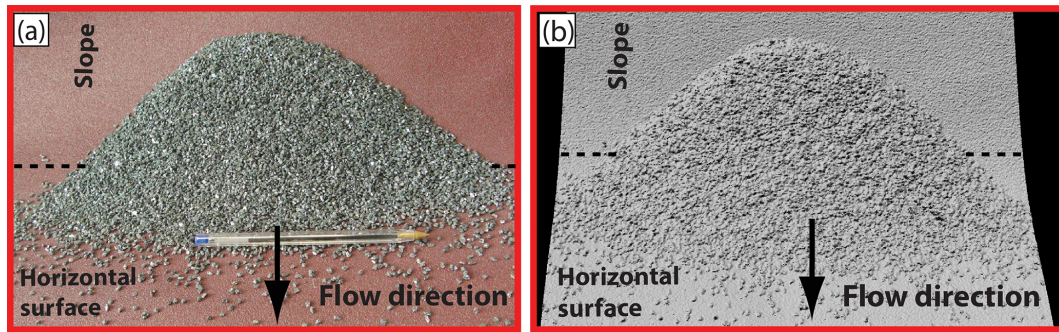


**Figure 3.** (a) Photography of a deposit of coarse granular material; (b) 3-D model of the deposit obtained by 3-D laser scanning.

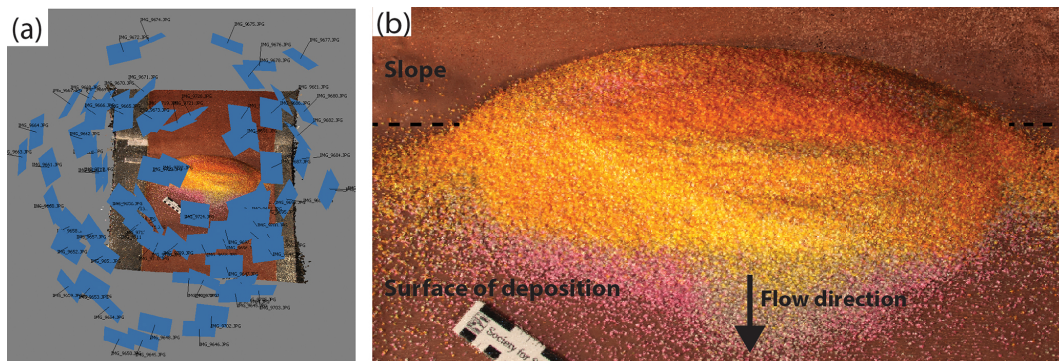


**Figure 4.** (a) View of the different position of the camera to take pictures for structure-from-motion photogrammetry; (b) 3-D model obtained with structure from motion. Three colored sands were used for this experiment (yellow, grey, pink).

ing filters are used in preprocessing steps (Gonzalez and Woods, 2002; Pugazhenti and Priya, 2013). After Gonzalez and Woods (2002), order-statistic filters are non-linear filters whose response is based on ordering the pixel contained in the image area encompassed by the filter and then replacing the value of the center pixel with the value determined by the ranking value. The first step was to remove the noise using 2-D median filtering using different window sizes (Fig. 5b and c).

#### (b) Application of a gradient operator

Once the noise was removed from the dataset obtained with the 3-D digitizer or SfM, a numerical gradient was applied to the filtered dataset. The gradient was applied along two directions to highlight changes in the slope orientation as proposed in Kumar et al. (1996) and Gonzalez and Woods (2002). We first calculated the gradient parallel to the flow direction (along the  $x$  axis) and then the gradient perpendicular to the flow direction (along the  $y$  axis):

$$\nabla F = \frac{\partial F}{\partial x} i + \frac{\partial F}{\partial y} j. \quad (1)$$

The objective of detecting variation of the gradient along  $x$  and  $y$  is to highlight any preferential orienta-

tion. The detected variations of the slope are interpreted as structures developed on the surface of the deposit. Once the gradient operator is applied, the point cloud is imported in the IMInspect module of PolyWorks software (InnovMetric)

#### (c) Comparison with real case

In order to extend the proposed workflow to a real case study, we decided to apply the filtering gradient operator techniques to the well-known Frank Slide event (Alberta, Canada). This deposit presents several geometrical features, which are mainly longitudinal and perpendicular to the flow direction (Longchamp et al., 2011; Charrière et al., 2015).

## 4 Results

### 4.1 Results I: experiment description

#### (a) Visual inspection from photography

Laboratory experiments were carried out using different volumes, grain sizes, and different basal roughness, but only the finer grain size (F120) presented visible features on the surface of the deposit as shown in Fig. 6a. Three distinct sets of features can be observed



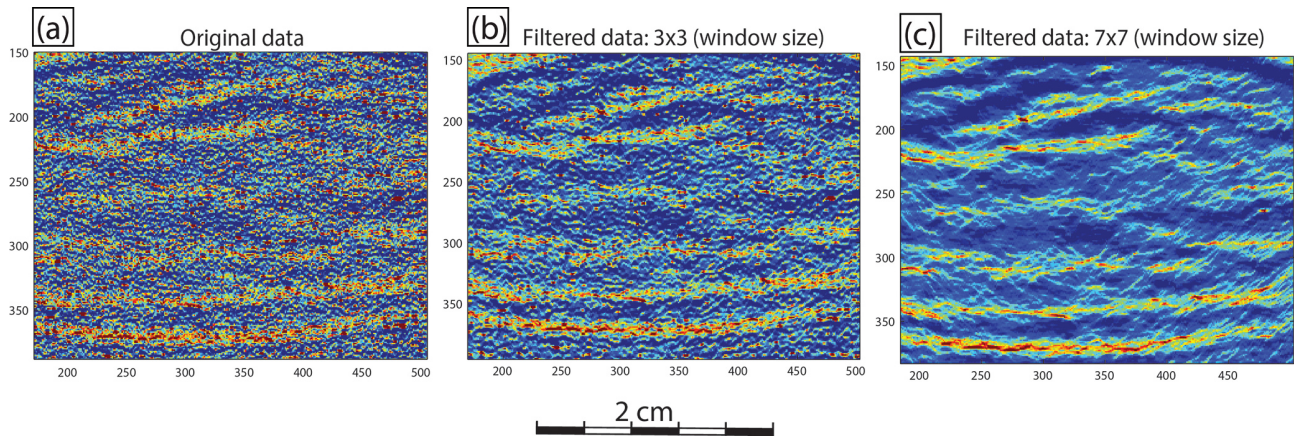


**Figure 5.** Application of the median filter to remove noises. (a) Original data; (b) filtered data with a  $3 \times 3$  window size; (c) filtered data with a  $7 \times 7$  window size.

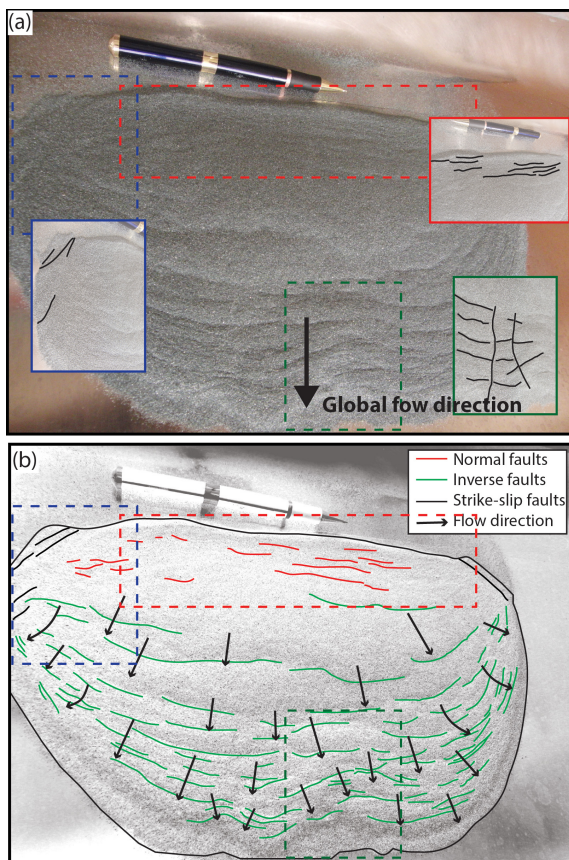


**Figure 6.** (a) Analog deposit (F120, aluminum substratum), view from the top; (b) result visual inspection and feature mapping observed on the deposit surface.

in this figure: inverse faults, normal faults, and strike-slip faults. The first set, the inverse faults, is composed of long features, perpendicular to flow direction following the outline of the front with a tendency to become

parallel to the global flow direction at the lateral margins (green lines in Fig. 6b). The second set is formed by thin normal faults located at the rear part of the deposit and perpendicular to the flow direction (red lines in Fig. 6b). Two different sets of strike-slip faults can be observed. The first one is composed of short and thin features parallel to the flow direction and present at the front of the deposit. These features can be observed cutting the inverse faults at the frontal part and cutting the normal faults at the rear part. The second one is made of strike-slip faults parallel to the flow direction and present at the lateral margins of the deposit.

#### (b) Visual inspection from high-speed video

In high-speed video, propagation of the mass is easily observable. Sand of three different colors was used and was poured in the starting box as follow: 150 mL of red sand as the lower layer, 150 mL of grey sand as the intermediate layer, and finally 150 mL of green sand. The slope is made rough with the finer substratum ( $\mu = 33.40^\circ$ ), and the slope angle is  $40^\circ$ . Once the trap is open and the material is free to flow, all the layers are stretched under an extensional regime. Once the frontal part reaches the horizontal surface, its velocity is decreased. As the mass continues to flow on the slope, the front is compressed and pushed forward. The mass is finally stopped once all the mass reaches the horizontal surface. The high-speed video is available in the Supplement.

#### 4.2 Results II: point cloud processing

Figure 7 shows the results of the point cloud processing for all the simulations, i.e., using three grain sizes (F10, F36 and F120) on the different substrata (Table 2). For the coarser grain size (F10), the application of the different filters and

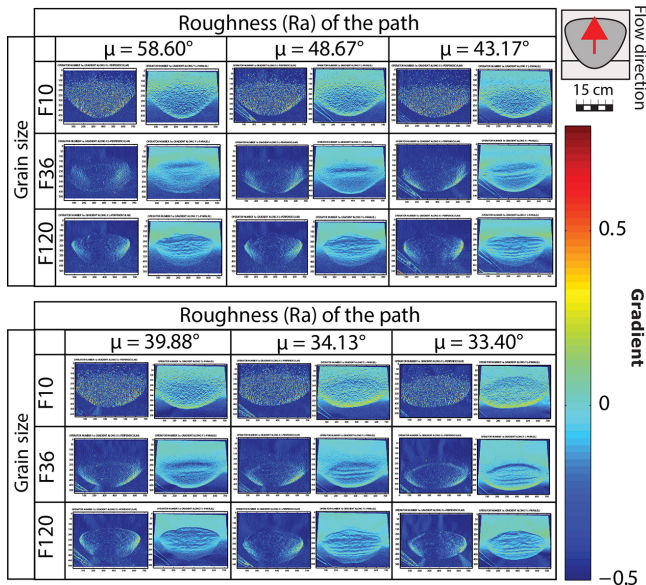


**Figure 7.** Results of the gradient along  $x$  and  $y$  applied to all experiments carried out for this research. The best results are obtained with the gradient along  $y$ . The influence of the grain size and the substratum on the shape of the deposit is clearly observable.

operator techniques has not highlighted any remarkable features. As the amplitude of the features is less than 1 mm, the coarser grain sizes are too large to capture deformation. The only noticeable thing is that the shape of the deposit became more ellipsoidal with a decreasing basal roughness and confirmed the observation made by Dufresne et al. (2016) that substrates shaped the morphology of rock avalanches. For the medium grain size (F36) the filters clearly highlighted a series of features perpendicular to the flow direction. In Fig. 7, it can also be observed that the basal friction influenced the formation of features at the deposit surface. The density of these features increases with the reduction of the basal roughness. In this case filters allowed detecting features that were not visible in the pictures alone.

As can be observed in Fig. 7, the gradient along  $y$  can be considered as an efficient manner of making observations of the different features affecting the surface of the deposits.

Using this operator, we observed that the back of the deposit presents high concentration of small features parallel to the flow direction. Figure 8a and b present the back of an analog deposit (F120 on the finest substratum) imported in the IMInspect module of PolyWorks software (InnovMetric) after processing the point cloud. Two different sets are observable: one perpendicular to the flow direction and the second composed of features parallel to the flow direction and cutting the first set (Fig. 8). The first set was observed with the naked eye, whereas the second set is only recognizable after post-processing.

### 4.3 Frank Slide

The same visual inspection and filtering methods were applied to the Frank Slide deposit. Figure 9a is the result of the interpretation of the features mapped directly in the digital elevation model (DEM), and Fig. 9b is the result of the application of a gradient along the flow direction. The main features observed in the DEM are also recognizable on the gradient map, but a series of structures that are masked on the DEM image can be identified in the gradient image. Figure 9c and d show a zoom of the deposit after the filtering. In Fig. 9c, features parallel to the flow direction are clearly identifiable, whereas in Fig. 9d the features are parallel to the flow direction.

## 5 Discussion

Our workflow has allowed the identification of three distinct sets of features on the analog granular flow deposit. Those features are important marks of the processes happening during the flow and the emplacement of the mass and could be crucial in improving our understanding of the dynamics and the reasons for the high mobility of rock avalanches. The inverse faults are well marked on the deposit front, reflecting the compression affecting the frontal part of the mass. An inverse faulting system appears as soon as the frontal part of the granular mass hits the surface of deposition and its velocity starts to slow down. Then, the granular material accumulates on the rear part, pushing forward and compressing the frontal part of the deposit. Normal faults were formed during an extensional regime when the mass was stretched during the flow and by the pulling of the frontal part of the mass. Strike-slip faults are present at the front of the deposit. As the mass is thinner at the margins, consequently the velocity decreases while the central part of the mass is still in motion, allowing strike-slip faults to appear at the lateral margins of the deposit. The strike-slip faults are the expression of the shearing that occurred during the deceleration of the mass (Shea and van Wyk de Vries, 2008).

Thanks to the application of the filtering on analog deposit 3-D datasets, the structures observed during the laboratory experiments were highlighted. One advantage is that the use of filters allows detecting features for the finest sand (F120) and also for the medium one (F36), for the totality of the basal roughness. The fact that no features are observed for the coarse grain size (F10) can be explained by the fact that the size of the features is on the same order of magnitude as the size of the grains. The gradient along  $y$  gave the best results since it allowed detecting long inverse faults at the front and some normal faults at the back. Moreover, the study of the result of the  $y$  gradient with the PolyWorks software shows that the normal faults at the back are numerous and cut by strike-slip faults (Fig. 8). These strike-slip faults appear after the extensional regime, during the shearing caused by the mass deceleration. These features give crucial informa-



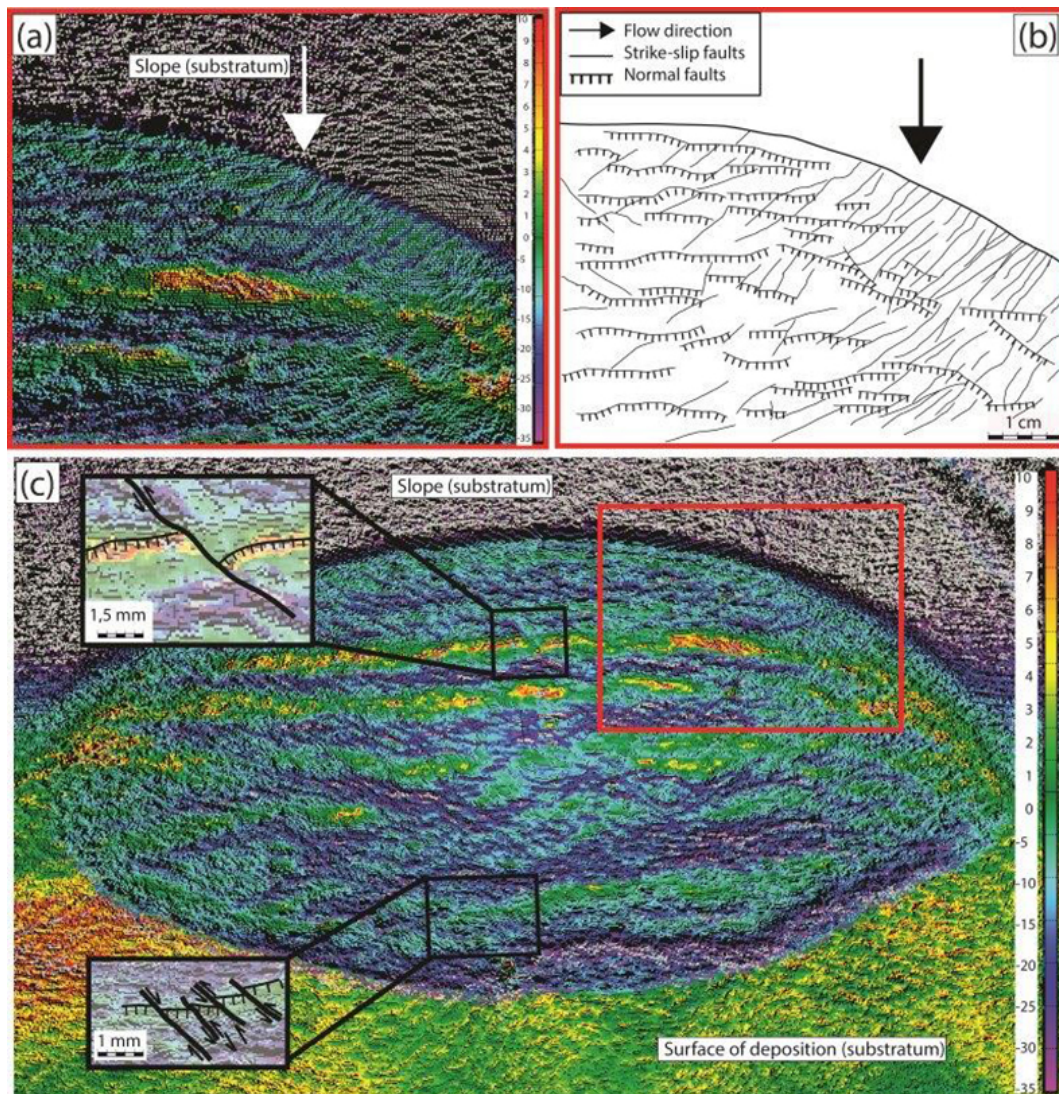


**Figure 8.** (a) Portion of the back of a deposit after post-processing and (b) detailed mapping of the back of the deposit. Strike-slip faults are numerous at the back, cutting normal faults. (c) The whole result.

tion on the mobility of the mass and are not detectable with the naked eye.

Thus, different regimes were distinguished: the compressional, the extensional and the shearing regimes. Based on this assumption, we could deduce the behavior of the granular mass by looking at the high-speed camera snapshots as shown in Fig. 10. This figure represents for each time step on the one hand the movie snapshot and on the other the interpretation related to it. In order to improve the clarity of the observation made, no distinction between the layers is made for the interpretation. Two main regimes are detected: the compressional one, outlined on the interpretation with dots, and the extensional one, outlined with lines. Following the time steps shown in Fig. 10 we can then observe the following:

- Step 1: Once the trap is open, the front of the granular material starts to flow. Because of the release geometry, layering occurred during the flow.
- Step 2: All the mass behaves under an extensional regime through all directions during the time preceding the deposition of the granular flow.
- Step 3: Shortly after the free flow, the front of the mass hits the surface of deposition, suddenly decreasing its velocity. Two different tensional states are found at this step. While the mass on the slope is under a high extensional regime, the front starts to be under a compressional regime as it hits the surface of deposition and the velocity starts to slow down. In addition to that, at this stage of the experiment, we start observing one additional aspect characterizing the green layer. In fact we



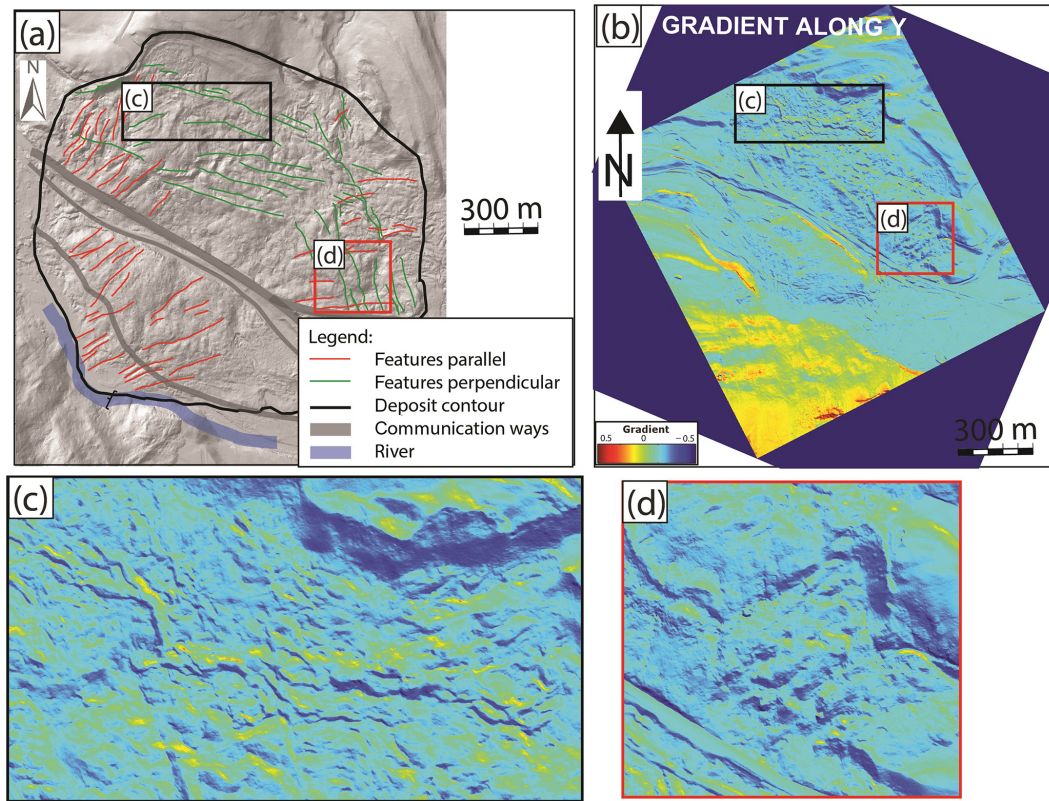


**Figure 9.** (a) Map of the different features observed in the DEM of the Frank Slide deposit; (b) result of the gradient along  $y$  applied to the DEM of Frank Slide; (c) zoom on features perpendicular to the flow direction; (d) zoom on features parallel to the flow direction.

can first distinguish a part of the green mass flowing which behaves differently from the rest of the mass. This part is likely to constitute the rear zone in the initial configuration of this layer. Moreover, at this step, it can be observed that the basal red layer has a lower velocity than the other layers, as it is less visible in the picture.

**Step 4:** At this step, the back is still under an extensional regime and the front under a high compressive regime as the flowing material continues to push it forward. The rear part of the green layer is faster than the underneath layers.

**Step 5:** The grey and green layers continue to be pushed by the main body of the mass. Consequently, shearing appears at the front. As the red layer is the basal layer, it is slowed by friction. As the margins of the mass are thinner compared to the central part, their velocity is less important, and shearing takes place. Simultaneously, the rear part of the green layer is faster compared to the lower layers and hits the mass already deposited.

**Step 6:** The back of the mass continues to flow and is still under an extensional regime, pushing the front forward. At this step, shearing is still important at the margins and at the front.

**Step 7:** The front is stopped, and the rest of the material still on the ramp finishes flowing down, creating the shearing observed at the back of the deposit and cutting the normal faults.

**Step 8:** The mass is finally stopped. It is interesting to highlight that the original stratigraphy is conserved and observable at the front.

The profile AA' along the flow direction was obtained for the laboratory experiment (Fig. 11a). This profile allowed observing the internal part of the mass and the depth of the main features. Figure 11b gives the image of the section along the AA' line shown in Fig. 11a, and Fig. 11c is its interpretation. In Fig. 11c, inverse faults are visible at the front (well marked by red grains in Fig. 11b) whereas normal faults are visible at the rear part of the deposit. In this figure, it can be observed that the center of the mass is mainly composed of green sand, confirming that the rear part of the green layer in Fig. 10 hits the mass already present on the surface of deposition (steps 5–7 in Fig. 10). When this mass hits the deposit, it probably increased the compression, explaining the numerous inverse faults present at the front (Fig. 11c).

To confirm what was observed, the number of colored sand grains has been counted along the central section of the deposit, as reported on Fig. 12. Results confirmed what

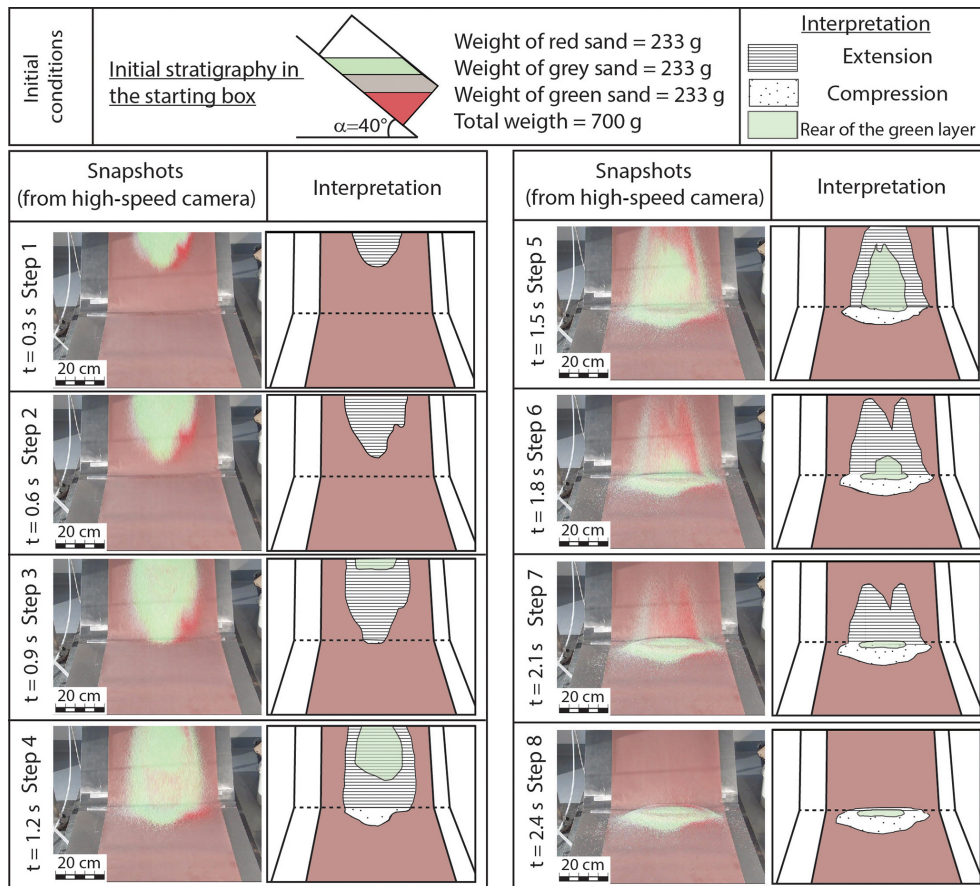


**Figure 10.** Time lapse of an analog granular flow (0.3 s between each picture). Three colored sands were used during this experiment (red, grey, green). In the left column are the snapshots of the experiment, and in the right column the interpretation of the flowing mass.

is shown by Fig. 11b and c with the identification of an extension-dominated area in the rear and a compression-dominated area in the front. The rear part of the deposit corresponds to the extension-dominated area. This area is mainly composed of red sand, whereas few green grains were observed. In contrast, the central part of the deposit is mainly composed of green sands. Indeed, this part corresponds to the rear part of the deposit that hit the mass already deposited (Fig. 10). The frontal part of the deposit corresponds to the compression-dominated area. The compression caused by the impact of the green layer of grains in the central part pushed part of the lower layer (red) further on the front and towards the surface, creating the inverse faults also shown in Fig. 11c. Indeed, in this frontal part, we can observe that the amount of red sand increases.

Because of the position of the profile, the red layer is not clearly visible at the front of Fig. 11b and 11c, but the conservation of the initial stratigraphy is observable in Fig. 11a. The fact that the initial stratigraphy is preserved in the final deposit is relevant since this feature has already been detected in several real cases, and it has been recognized as one of the main ones characterizing rock avalanche deposit (Eris-

mann, 1979; Manzella and Labiouse, 2013). Thanks to the film analysis we could then relate some propagation mechanisms to the consequent preservation of the initial stratigraphy in the final deposit, and this could give insight into the dynamics of real rock avalanches.

This study confirmed that the structures are not randomly distributed. As can be observed in Fig. 6, the inverse faults are present at the frontal part of the deposit, which corresponds to the compression-dominated area. Normal faults are mainly observed at the back of the deposit (Figs. 6 and 8), which corresponds to the extension-dominated area. Finally, strike-slip faults are observed at the back and at the margins of the deposit (Figs. 6 and 8). These repartition was also observed in the Blackhawk deposit (Fig. 1a) and in a Martian deposit (Fig. 1b) (Shea and van Wyk de Vries, 2008). Based on the study of the DEM of the Frank Slide deposit and with the filtering technique, the same repartition of the features was observed (Fig. 9).



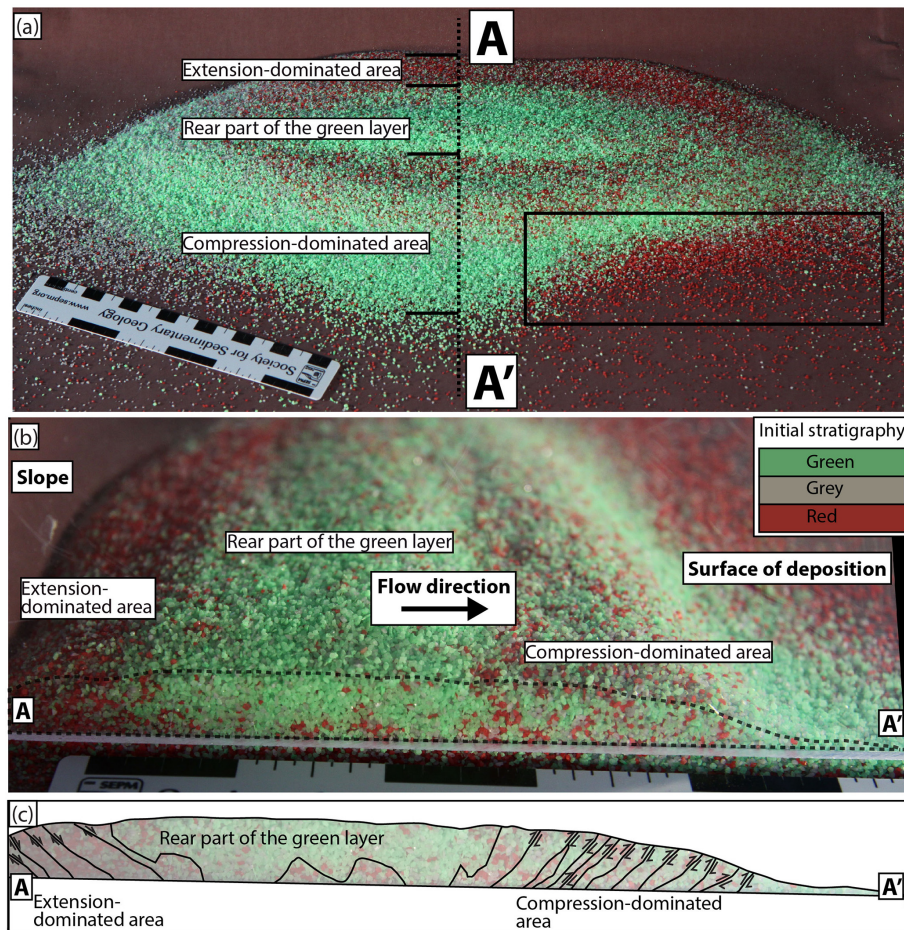


**Figure 11.** (a) Analog result of the experiment carried with three colored sands (Fig. 10); (b) cross section AA' through the center of the analog deposit; (c) interpretation of the cross section AA'.

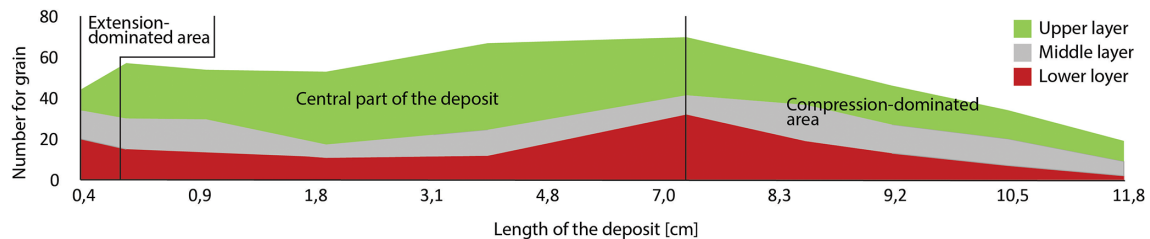


**Figure 12.** Repartition of the colored sand grains within the deposit.

## 6 Conclusions

The use of a 3-D dataset, accurate visual inspection, and a performing filtering method provide crucial information on the motion of granular mass. We summarize as follows:

1. Three families of faults were highlighted on the surface of the deposit: normal faults, inverse faults, and strike-slip faults. We also highlighted that strike-slip faults are present at the back of the deposit.
2. The identification of the different features allowed identifying three regimes during the propagation of the mass: extensional, compressional and shearing. The extension to real cases of the interpretation of the motion of the granular mass based on laboratory experiments is confirmed by the fact that the initial stratigraphy is preserved in both cases, and this is an important characteristic of rock avalanche deposits.
3. The result of the filters on the 3-D dataset is a colored point cloud where the slope variations are assigned to

a color scale. The method is fast and results in a rapid mapping of the deposit.

4. The use of a laser scanner and structure-from-motion photogrammetry are two different techniques of obtaining a 3-D dataset. Both are valid, and often they wind up being complementary.
5. Even if the simulated roughness is not realistic compared to realistic conditions, it gives good insight into how the basal roughness influence the motion.
6. The analog deposits present similar features to real cases events (Blackhawk and Martian deposits, Fig. 1).
7. The proposed methodology to map the deposit is fast, easy to use, and cheap.

The application of the filtering technique on the deposit of the Frank Slide rock avalanches gives encouraging results and after some further improvements could be applied in the future to help gain an understanding of the dynamics of emplacement of historic rock avalanche observing their deposit features.

**The Supplement related to this article is available online at doi:10.5194/esurf-4-743-2016-supplement.**

**Acknowledgements.** The authors are grateful to P.-E. Cherix for the design of the laboratory setup and to Martin Boesinger for his precious help in laboratory. The authors are also grateful to the Alberta Geological Service for providing the data of the Frank Slide. Finally, many thanks to the reviewers, editor, and associate editors for the helpful comments.

Edited by: T. Coulthard

Reviewed by: two anonymous referees

## References

- Adams, T., Grant, C., and Watson, H.: Simple algorithm to relate surface roughness to equivalent sand grain roughness, *Int. J. Mech. Eng. Mechatr.*, 1, 2929–2724, 2012.
- Andrade, S., van Wyk, D., and de Vries, B.: Structural analysis of the early stage of catastrophic stratovolcano flank-collapse using analogue models, *B. Volcanol.*, 72, 771–789, 2010.
- Charrière, M., Humair, F., Froese, C., Jaboyedoff, M., Pedrazzini, A., and Longchamp, C.: From the source area to the deposit: collapse, fragmentation and propagation of the Frank Slide, *GSA Bull.*, 128, 332–351, 2015.
- Cruden, D. M. and Hungr, O.: The debris of the Frank Slide and theories of rockSlide-avalanche mobility, *Can. J. Earth Sci.*, 23, 425–432, 1986.
- Davies, T. R.: Spreading of rock avalanche debris by mechanical fluidization, *Rock Mech.*, 15, 9–24, 1982.
- Davies, T. R. H. and McSaveney, M. J.: Runout of dry granular avalanches, *Can. Geotech. J.*, 36, 313–320, 1999.
- Davies, T. R. H. and McSaveney, M. J.: Runout of rock avalanches and volcanic debris avalanches, *Proc. Int. Conf. Fast Slope Movem.*, Naples, 2, 11–13, 2003.
- Dufresne, A.: Granular flow experiments on the interaction with stationary runout path materials and comparison to rock avalanche events, *Earth Surf. Proc. Land.*, 37, 1527–1541, 2012.
- Dufresne, A. and Davies, T. R.: Longitudinal ridges in mass movement deposits, *Geomorphology*, 105, 171–181, 2009.
- Dufresne, A., Prager, C., and Bösmeyer, A.: Insights into rock avalanche emplacement processes from detailed morphological studies of the Tschirgabt deposit (Tyrol, Austria), *Earth Surf. Proc. Land.*, 41, 587–602, 2016.
- Erismann, T. H.: Mechanisms of large landslides, *Rock Mechanics Felsmechanik*, 12, 15–46, 1979.
- Francis, P. W., Gardeweg, M., O’Callaghan, L. J., Ramirez, C. F., and Rothery, D. A.: Catastrophic debris avalanche deposit of Socoma volcano, north Chile, *Geology*, 14, 600–603, 1985.
- Friedman, S. J., Kwon, G., and Losert, W.: Granular memory and its effect on the triggering and distribution of rock avalanche events, *J. Geophys. Res.*, 108, B82380, doi:10.1029/2002JB002174, 2003.
- Gonzalez, R. C. and Woods, R. E.: *Digital Image Processing – Sec. Ed.*, Prentice-Hall, Inc., 2002.
- Heim, A.: *Der Bergsturz und Menschenleben*, Fretz und Wasmuth Verlag, Zürich, 218 pp., 1932.
- Hsü, K. J.: Catastrophic debris streams (strurzstroms) generated by rockfall, *Geol. Soc. Am. Bull.*, 86, 129–140, 1975.
- Hungr, O., Evans, S. G., Bovis, M., and Hutchinson, J. N.: Review of the classification of landslides of the flow type, *Environ. Eng. Geosci.*, 22, 221–238, 2001.
- Iverson, R. M. and Denlinger, R. P.: Flow of variably fluidized granular masses across three-dimensional terrain. I. Coulomb mixture theory, *J. Geophys. Res. B*, 106, 537–552, 2001.
- Kelfoun, K. and Druitt, T. H.: Numerical modelling of the emplacement of Socoma rock avalanche, Chile, *J. Geophys. Res.*, 110, B12202, doi:10.1029/2005JB003758, 2005.
- Kumar, L., Skidmore, A. K., and Knowles, E.: Modelling topographic variation in solar radiation in a GIS environment, *Int. J. Geogr. Inf. Sci.*, 11, 475–497, 1996.
- Locat, P., Couture, R., Leroueil, S., Locat, J., and Jaboyedoff, M.: Fragmentation energy in rock avalanches, *Can. Geotech. J.*, 43, 830–851, 2006.
- Longchamp, C.: *The Propagation of Unconstrained Dry Granular Flows: from Laboratory to Numerical Modélisation*. PhD Thesis, University of Lausanne, Switzerland, 2016.
- Longchamp, C., Charrière, M., and Jaboyedoff, M.: Experiments on substratum roughness, grain size and volume influence on the motion and spreading of rock avalanches, *Pan-Am CGS Geotechnical Conference*, 2001.
- Manzella, I.: *Dry rock avalanche propagation: unconstrained flow experiments with granular materials and blocks at small scale*, PhD thesis, EPFL, 2008.
- Manzella, I. and Labiouse, V.: Qualitative analysis of rock avalanches propagation by means of physical modelling of not constrained gravel flows, *Rock Mech. Rock Eng.*, 41, 133–151, 2008.



- Manzella, I. and Labiouse, V.: Flow experiments with gravel and blocks at small scale to investigate parameters and mechanisms involved in rock avalanches, *Eng. Geol.*, 109, 146–158, 2009.
- Manzella, I. and Labiouse, V.: Empirical and analytical analyses of laboratory granular flows to investigate rock avalanche propagation, *Landslides*, 10, 23–36, 2013.
- McDougall, S. and Hungr, O.: A model for the analysis of rapid landslide motion across three-dimensional terrain, *Can. Geotech. J.*, 41, 1084–1097, 2004.
- Nicoletti, P. G. and Sorriso-Valvo, M.: Geomorphic controls of the shape and mobility of rock avalanches, *Geol. Soc. Am. Bull.*, 103, 1365–1373, 1991.
- Paguican, E. M. R., van Wyk de Vries, B., and Lagmay, A.: Hummocks : how they form and how they evolve in rockslide-debris avalanches, *Landslides*, 11, 67–80, 2014.
- Pedrazzini, A., Froese, C. R., Jaboyedoff, M., Hungr, O., and Humair, F.: Combining digital elevation model analysis and run-out modeling to characterize hazard posed by a potentially unstable rock slope at Turtle Mountain, Alberta, *Can. Eng. Geol.*, 128, 76–94, 2012.
- Pugazhenti, D. and Pria K.: A quantitative approach for textural image segmentation with median filter, *Int. J. Adv. Res. Tech.*, 2, 1–5, 2007.
- Scheidegger, A. E.: On the prediction of the reach and velocity of catastrophic landslides, *Rock Mech. Rock Eng.*, 5, 231–236, 1973.
- Shea, T. and van Wyk de Vries, B.: Structural analysis and analogue modeling of the kinematics and dynamics of rockslide avalanches, *Geosphere*, 4, 657–686, 2008.
- Van Gassen, W. and Cruden, D. M.: Momentum transfer and friction in the debris of rock avalanches, *Can. Geotech. J.*, 26, 623–628, 1989.
- van Wyk de Vries, B., Self, S., Francis, P. W., and Keszthelyi, L.: A gravitational spreading origin for the Socompa debris avalanche, *J. Vol. Geotherm. Res.*, 105, 225–247, 2001.
- Westboy, M. J., Brasington, J., Glasser, N. F., Hambrey, M. J., and Reynolds, J. M.: “Structure-from-Motion” photogrammetry: A low-cost, effective tool for geoscience applications, *Geomorphology*, 179, 300–314, 2012.